Mechanical Systems and Signal Processing 224 (2025) 112002

Contents lists available at ScienceDirect

Mechanical Systems and Signal Processing

journal homepage: www.elsevier.com/locate/ymssp

Application of thermoelasticity in the frequency-domain multiaxial vibration-fatigue criterion

Jaša Šonc, Klemen Zaletelj, Janko Slavič *

University of Ljubljana, Faculty of Mechanical Engineering, Aškerčeva 6, 1000 Ljubljana, Slovenia

ARTICLE INFO

Communicated by S. Fassois

Keywords:
Thermoelasticity
Multiaxial criterion
Vibration fatigue
Modal decomposition

ABSTRACT

In vibration fatigue, high-spatial-density experimental damage identification is hard to conduct. Fatigue damage is typically localized (in time and space) and loads can change direction with time. Thermoelasticity studies the interaction between temperature changes and elastic deformations in materials: minute changes in temperature can be related to the sum of the normal stresses, providing information about the multiaxial stress state. This research discusses the application of thermoelasticity in multiaxial criterion resulting in the equivalent uniaxial load. In this research, the thermoelasticity-based equivalent uniaxial load is related to the established theory on vibration-fatigue damage estimation in the spectral domain. The introduced thermoelasticity-based criterion is compared to the Equivalent von Mises stress criterion. Building on theoretical, numerical, and experimental research, this work examines the limitations of thermoelasticity-based criterion. Where the surface shear stresses are significantly smaller than the normal stresses, the numerical and experimental research shows promising results.

Based on the introduced thermoelastic multiaxial criterion and with the recent progress in thermal imaging and signal processing, new possibilities for a close-to-real-time full-field fatigue-damage estimation open up.

1. Introduction

Vibrating structures are prone to failure because of material fatigue, especially when excited at, or close to, one of their eigenfrequencies [1,2]. Different approaches and methods are available for vibration-fatigue analysis. They can be defined in the time- or frequency-domain. Frequency-domain methods are preferred when the excitation is random and only the statistical distribution of the excitation is known [3]. This is applicable in structural dynamics, where the random excitation is usually provided in terms of Power Spectral Density (PSD) functions. Multiaxial, non-Gaussian and non-stationary excitation [4–7] and their influence on fatigue life [8,9] have been extensively researched in recent years. Fatigue damage can also be related directly to the dynamic properties of a structure by using the modal decomposition, which greatly reduces the calculation times [10,11]. For uniaxial loads, different damage-estimation methods using spectral moments have been developed, such as: Dirlik [12], Tovo–Benasciutti [13], Gao–Moan [14], Petrucci–Zuccarello [15], Zhao–Baker [16]. For a review of more than 20 methods, see [17]. The material parameters for high-cycle fatigue (S-N curve) are defined for uniaxial stress states [1]. Thus, for the multiaxial stress states, the response stress tensor must be converted into the uniaxial equivalent stress. For this, several multiaxial vibration-fatigue criteria are available. In structural dynamics, the criteria defined in the frequency-domain are especially interesting [18–20]; for

* Corresponding author.
E-mail address: janko.slavic@fs.uni-lj.si (J. Slavič).

https://doi.org/10.1016/j.ymssp.2024.112002
Received 8 July 2024; Received in revised form 19 September 2024; Accepted 28 September 2024

Available online 7 October 2024

comparison studies, see [21,22]. In the last year, several new approaches have been researched. Schmidt and Kraft [23] proposed the linear-wave-interference equivalent-stress method, which is based on the complex invariant. Aime et al. [24] researched the fatigue-damage multi-spectrum and extreme-response multi-spectrum. Sui et al. [25] researched, by analogy to the Projection-by-Projection criterion, an improved fatigue-response spectrum method. Despite the recent efforts in multiaxial criteria, the frequency-domain formulation of the equivalent von Mises stress (EVMS), as defined by Preumont et al. [26], is still frequently used. A drawback of the EVMS is that it disregards the phase angles between the normal and shear stresses, so it is only valid if they are in phase [27,28].

If the theoretical methods to describe the multiaxial loads see great progress, we see relatively little progress in the field of identifying fatigue damage; potentially real-time and full-field. In recent years there has been an increasing utilization of non-contact full-field measurement techniques in structural dynamics [29,30]. Cameras based in the visible spectrum can be used for measuring displacements and deformations [31] and also for image-based experimental modal analysis [32]. For a vibration-fatigue estimation, the strain mode shapes are required. To identify strain shapes with the visible-spectrum camera, the relationship between displacement and strain must be known. For the Euler–Bernoulli beam, the second spatial derivative of the measured displacement must be calculated [33], which greatly increases the noise level [34]. Displacements must also be in-plane, as the out-of-plane displacements are not detected with a traditional setup (multiple cameras [35] and frequency-domain triangulation [36] enable out-of-plane measurement).

In contrast to conventional cameras, cameras operating in the infrared (IR) spectrum do not require any pattern or lighting, since measurements are not based on displacement identification but rather directly on stress-induced temperature differences. However, some measures have to be taken to minimize the IR reflection from surroundings and background IR radiation [37]. Furthermore, thermal cameras take advantage of the thermoelastic effect to measure the stress (also known as Thermoelastic stress analysis (TSA) [37]). Knowing the Young's modulus, the strain shapes are obtained without spatial derivations. Stress caused by out-of-plane displacements can be measured as well [33].

Thermoelastic stress analysis is an experimental method that uses various types of infrared sensors to determine the stresses on the surfaces of materials [37,38]. The fundamental theory upon which it operates is long known [39,40]; however, it has only recently become applicable in various fields, due to the advances in technology for detecting small temperature changes at the level of a fraction of a mK at relatively high frequencies [41,42].

High-speed, infrared thermal cameras that are capable of achieving sampling frequencies up to several kHz have been successfully used to identify strain mode shapes using the thermoelastic principle [33,43] and also to determine the spatial damage-intensity distribution of the excited modes [44] with the modal decomposition method [10].

When a thermal camera is used for measuring multiaxial stresses on the surface of a structure, it provides a scalar value directly, *i.e.*, the sum of the normal stresses, while disregarding the shear stresses. This conversion from the full tensor to the scalar value is similar to the calculation of the uniaxial equivalent stress, as done in vibration-fatigue analysis [45]. There is currently a limited understanding of using thermoelasticity-based measurements in multiaxial vibration fatigue in comparison to other methods. Therefore, in this research, a new multiaxial vibration-fatigue criterion based on thermoelasticity is introduced. The criterion sums the normal stresses of a stress response, and uses the obtained uniaxial equivalent stress for vibration-fatigue analysis. By doing so, the damage that would be identified with a thermal camera is simulated. A numerical experiment is conducted in which the proposed criterion is compared to the established EVMS, as the structure is excited with a broadband random signal. The experimental research compares the numerical findings to a real case.

This research is organized as follows. The theoretical background for the vibration fatigue, structural dynamics and thermoelasticity is given in Section 2. The proposed thermoelastic multiaxial damage criterion is presented in Section 3. Section 4 describes a numerical experiment using the proposed criterion, and a real experiment with the thermal camera. In Section 5, the results from the numerical and real experiments are compared and discussed. The last section draws the conclusions.

2. Theoretical background

2.1. Thermoelastic effect

The thermoelastic effect describes the relation between the stress state and the temperature difference that occurs in materials during loading [39,40]. Under adiabatic conditions, local heating under compression and local cooling under expansion can be observed. During harmonic excitation, the harmonic stresses in a solid material produce a harmonic temperature response, related to the first stress invariant (*i.e.*, the sum of the normal stresses) [46]. The amplitude of the temperature variations are typically of the order of mK. Two conditions are required to achieve an adiabatic process. First, the deformations must be within the elastic range; second, the reversibility of the process must be achievable, *e.g.*, the process must occur fast enough so the heat dissipation to the surroundings and other parts of the material is negligible [43]. For metals, the adiabatic conditions are achieved at a few Hz of harmonic excitation (*e.g.*, aluminium at 5 Hz) [47], which means that the adiabatic condition is generally satisfied for applications in structural dynamics [33]. For adiabatic conditions and isotopic materials, the thermoelastic effect is defined as (for details, see Appendix):

$$\Delta\sigma_{kk} = -\Delta T \frac{\rho}{\alpha T_0} c_p \tag{1}$$

or:

$$\Delta T = K_m \left(\Delta\sigma_{xx} + \Delta\sigma_{yy} + \Delta\sigma_{zz}\right) \tag{2}$$

where $\Delta\sigma_{kk}$ represents the sum of the change of the normal stresses in all three directions ($\Delta\sigma_{xx}, \Delta\sigma_{yy}, \Delta\sigma_{zz}$) and K_m is the thermoelastic constant [48]:

$$K_{\mathrm{m}} = -\frac{\alpha\, T_0}{\rho\, c_{\mathrm{p}}} \tag{3}$$

T_0 is the temperature of the surroundings and α is the coefficient of heat expansion.

2.2. Stress response of MDOF systems

Vibration fatigue is generally related to continuous elastic structures. With the exception of very simple structures that can be described analytically, geometrically complex structures have to be defined with a system of differential equations, assuming hysteresis damping and N-degrees of freedom (MDOF). In real-world cases, MDOF systems theory is often applied to the finite element models, that enable effective and accurate analysis of complex structures. The system of equations can be written in matrix form [49]:

$$\mathbf{M}\,\ddot{\mathbf{x}}(t) + \mathrm{i}\,\mathbf{D}\,\mathbf{x}(t) + \mathbf{K}\,\mathbf{x}(t) = \mathbf{f}(t), \tag{4}$$

where $\mathbf{x}(t)$ and $\ddot{\mathbf{x}}(t)$ are the displacement and the acceleration vectors, respectively. $\mathbf{M}$, $\mathbf{D}$ and $\mathbf{K}$ are the mass, damping and stiffness matrices, respectively. $\mathbf{f}$ is the vector of the excitation forces. By assuming a harmonic excitation $x(t) = \mathbf{X}\,e^{\mathrm{i}\,\omega t}$ and a harmonic response $f(t) = \mathbf{F}\,e^{\mathrm{i}\,\omega t}$, where ω is the angular frequency and $\mathbf{X}$, $\mathbf{F}$ are the complex vectors of the response and excitation amplitudes. For harmonic conditions, Eq. (4) can be rewritten as [50,51]:

$$\mathbf{X} = \underbrace{\left(-\omega^2\,\mathbf{M} + \mathrm{i}\,\mathbf{D} + \mathbf{K}\right)^{-1}}_{\mathbf{H}(\omega)}\,\mathbf{F}, \tag{5}$$

where $\mathbf{H}(\omega)$ is the receptance matrix. Based on orthonormality [51], the receptance matrix $\mathbf{H}(\omega)$ is written in a diagonal form, where complex eigenvalues are defined as $\lambda_r^2 = \omega_r^2\left(1 + \mathrm{i}\eta_r\right)$. Diagonal dots $\ddots$ denote a diagonal matrix:

$$\mathbf{H}(\omega) = \boldsymbol{\Phi}\begin{bmatrix} \ddots & & \\ & \omega_r^2\left(1+\mathrm{i}\eta_r\right) - \omega^2 & \\ & & \ddots \end{bmatrix}^{-1}\boldsymbol{\Phi}^{\mathrm{T}} \tag{6}$$

ω_r is a natural frequency and η_r is the damping loss factor of the rth mode. The mass-normalized eigenvectors of a system are stacked in a matrix (each column corresponds to the rth vector). $\boldsymbol{\Phi} = \left[\boldsymbol{\phi}_1, \boldsymbol{\phi}_2, \ldots\right]$

The response obtained using the receptance matrix $\mathbf{H}(\omega)$ is in the form of displacements $\mathbf{X}(\omega)$. For the purpose of vibration-fatigue analysis, the stress response $\mathbf{X}_s(\omega)$ is required. From the rth displacement mode shape $\boldsymbol{\phi}_r$, the rth strain mode shape $\boldsymbol{\phi}_r^{\epsilon}$ is first obtained using the differential field operator $\overline{\mathbf{D}}$ [51]:

$$\boldsymbol{\phi}_r^{\epsilon} = \overline{\mathbf{D}}\,\boldsymbol{\phi}_r, \tag{7}$$

where:

$$\overline{\mathbf{D}} = \frac{1}{2}\left(\nabla + \nabla^{\mathrm{T}}\right) \tag{8}$$

The rth stress mode shape can be then obtained using Hooke's law, under the assumption of small displacements, by using the stiffness tensor $\mathbf{C}$:

$$\boldsymbol{\phi}_r^{s} = \mathbf{C}\,\boldsymbol{\phi}_r^{\epsilon} \tag{9}$$

Using these relations, the stress response to a given excitation can be calculated [51,52]:

$$\mathbf{X}^s(\omega) = \mathbf{C}\,\overline{\mathbf{D}}\,\mathbf{X}(\omega) = \underbrace{\boldsymbol{\Phi}^s\begin{bmatrix} \ddots & & \\ & \omega_r^2\left(1+\mathrm{i}\eta_r\right) - \omega^2 & \\ & & \ddots \end{bmatrix}^{-1}\boldsymbol{\Phi}^{\mathrm{T}}}_{\mathbf{H}_{sf}(\omega)}\,\mathbf{F}(\omega) \tag{10}$$

$\mathbf{H}_{sf}(\omega)$ is the stress frequency-response function (FRF) that can be written as a sum of the FRFs of all N modes:

$$\mathbf{H}_{sf}(\omega) = \sum_{r=1}^{N} {}_r\mathbf{H}_{sf}(\omega) = \sum_{r=1}^{N} \frac{{}_r\mathbf{A}_s}{\omega_r^2 - \omega^2 + \mathrm{i}\eta_r\omega_r^2}, \tag{11}$$

where ${}_r\mathbf{A}_s$ denotes the stress modal constants matrix for the rth mode [53]:

$${}_r\mathbf{A}^s = \begin{bmatrix} \phi^s_{1r}\phi_{1r} & \cdots & \phi^s_{1r}\phi_{jr} & \cdots & \phi^s_{1r}\phi_{N_{\mathrm{d}}r} \\ \vdots & \ddots & \vdots & \ddots & \vdots \\ \phi^s_{ir}\phi_{1r} & \cdots & \phi^s_{ir}\phi_{jr} & \cdots & \phi^s_{ir}\phi_{N_{\mathrm{d}}r} \\ \vdots & \ddots & \vdots & \ddots & \vdots \\ \phi^s_{N_{sr}}\phi_{1r} & \cdots & \phi^s_{N_{sr}}\phi_{jr} & \cdots & \phi^s_{N_{s}r}\phi_{N_{\mathrm{d}}r} \end{bmatrix}_{N_{\mathrm{s}}\times N_{\mathrm{d}},} \tag{12}$$

ϕ^s_{ir} and ϕ_{jr} represent the values of the stress modal shapes $\boldsymbol{\phi}^s_r$ and the displacement modal shapes $\boldsymbol{\phi}_r$, respectively. N_d and N_s denote the degrees of freedom of the modal displacements $\boldsymbol{\phi}_r$ and the modal stress shapes $\boldsymbol{\phi}^s_r$, respectively. To determine the system's response to random excitation, the power spectral density (PSD) of the stress response $\mathbf{S}_{ss}(\omega)$ is calculated, where $\mathbf{S}_{ff}(\omega)$ represents the PSD of the excitation force [51,54,55]:

$$\mathbf{S}_{ss}(\omega) = \mathbf{H}_{sf}(\omega) \cdot \mathbf{S}_{ff}(\omega) \cdot \mathbf{H}^{*\,\mathrm{T}}_{sf}(\omega), \tag{13}$$

where * denotes the complex conjugate. $\mathbf{S}_{ff}(\omega)$ is a matrix with a size of 3×3, while $\mathbf{S}_{ss}(\omega)$ has a size of 6×6.

In vibration-fatigue analysis the consideration of the full FEM model results in a large numerical problem [10]. However, as the solution in the frequency domain is usually limited to a smaller frequency range, only a subset of the natural frequencies denoted by M can be considered, which greatly reduces the calculation times, since the number of natural frequencies M is substantially smaller than the total number of natural frequencies N; the reduced FRF can be expressed as [10]:

$$\widetilde{\mathbf{H}}_{sf}(\omega) = \sum_{r=1}^{M} {}_r\mathbf{H}_{sf}(\omega) \tag{14}$$

If the natural frequencies are well separated from each other in the frequency domain, the power spectral density of the stress response can be approximated by [10]:

$$\widetilde{\mathbf{S}}_{ss}(\omega) = \widetilde{\mathbf{H}}_{sf}(\omega) \cdot \mathbf{S}_{ff}(\omega) \cdot \widetilde{\mathbf{H}}^{*\,\mathrm{T}}_{sf}(\omega) \approx \sum_{r=1}^{M} {}_r\mathbf{H}_{sf}(\omega) \cdot \mathbf{S}_{ff}(\omega) \cdot {}_r\mathbf{H}^{*\,\mathrm{T}}_{sf}(\omega) \tag{15}$$

Under the assumption that an individual mode only contributes to the damage in the vicinity of its own natural frequency, the following equation is obtained [10]:

$$\widetilde{\mathbf{S}}_{ss}(\omega) = \sum_{r=1}^{M} \frac{{}_r\mathbf{A}_s \cdot \mathbf{S}_{ff}(\omega) \cdot {}_r\mathbf{A}^{*\,\mathrm{T}}_s}{\omega^4 - 2\omega^2\omega_r^2 + \left(1+\eta^2\right)\omega_r^4} \tag{16}$$

2.3. Multiaxial criterion

For a vibration-fatigue analysis, the full response stress tensor must be converted into the uniaxial equivalent stress according to a selected criterion, which can later be used for a damage estimation [1,45]. The reason for this is that the vibration-fatigue analysis is based on the Palmgren–Miner hypothesis of linear damage accumulation [56,57], where the material properties for cyclic uniaxial stress states are known.

The stress state in the time domain can be described by the stress-tensor components:

$$\boldsymbol{\sigma}(t) = [\sigma_{xx}(t), \sigma_{yy}(t), \sigma_{zz}(t), \sigma_{xy}(t), \sigma_{xz}(t), \sigma_{yz}(t)]$$

Using the probabilistic approach in the frequency domain [21], the stress-tensor components are expressed through a PSD matrix $\mathbf{S}_{ss}(\omega)$ with a dimension of 6×6:

$$\mathbf{S}_{ss}(\omega) = \begin{bmatrix} S_{xx,xx}(\omega) & \cdots & S_{xx,yz}(\omega) \\ \vdots & \ddots & \vdots \\ S_{yz,xx}(\omega) & \cdots & S_{yz,yz}(\omega) \end{bmatrix}$$

The diagonal of this matrix contains the autospectral density functions, while the upper and lower triangular parts contain the cross-spectral density functions.

The multiaxial criteria in the frequency domain are frequently obtained as a reformulation of the criteria defined in the time domain and are classified in the following categories: critical plane criteria [45] and stress-invariant criteria [58]. For a review of multiple multiaxial criteria see, for example, Carpinteri et al. in [59] who reviewed the maximum normal or shear stress, normal strain on the fracture plane, maximum principal stress, Tresca and von Mises stress.

Generally, multiaxial criteria define the relation between the components of the stress tensor and the uniaxial equivalent stress. Depending on the type of criteria, the relation between a tensor and the equivalent stress can be linear or non-linear [60]. For criteria with linear relations (*e.g.*, maximum normal stress or strain, maximum shear stress), the same types of criteria that are used in the time domain can be used on the PSD in the frequency domain; The equivalent stress PSD can be calculated as a linear combination of the stress PSD components [60]. Non-linear criteria are defined by a non-linear relation in the time domain and need to be reformulated for use in the frequency domain. One of such criteria is the Preumont and Piéfort reformulation of the equivalent von Mises stress (EVMS) [21,26,61]. EVMS transforms the PSD of the stress tensor $\mathbf{S}_{ss}(\omega)$ into the PSD of the uniaxial equivalent stress [26]. For the reduced model, the EVMS is defined as [51]:

$$\widetilde{S}_c(\omega) = \sum_{r=1}^{M} {}_rS_c = \sum_{r=1}^{M} \mathrm{Trace}\left[\mathbf{Q} \cdot {}_r\mathbf{S}_{ss}(\omega)\right], \tag{17}$$

where $\mathbf{Q}$ is a constant matrix:

$$\mathbf{Q} = \begin{bmatrix} 1 & -1/2 & -1/2 & 0 & 0 & 0 \\ -1/2 & 1 & -1/2 & 0 & 0 & 0 \\ -1/2 & -1/2 & 1 & 0 & 0 & 0 \\ 0 & 0 & 0 & 3 & 0 & 0 \\ 0 & 0 & 0 & 0 & 3 & 0 \\ 0 & 0 & 0 & 0 & 0 & 3 \end{bmatrix} \tag{18}$$

2.4. Vibration fatigue using spectral methods

In probabilistic approach to vibration fatigue, the value of damage intensity d is used instead of absolute damage value D, as the calculations are based in the frequency domain. The damage intensity represents the damage rate or damage per unit time and is given with the equation [51]:

$$d = \frac{D}{T}, \tag{19}$$

where T represents the fatigue life or the time after which the failure occurs. Note that D represents the amount of damage that denotes failure, which is usually 1, but can sometimes be chosen differently [51]. Most frequency-domain methods for vibration-fatigue analysis rely on spectral moments. To compute these spectral moments, the uniaxial equivalent of the stress PSD $\widetilde{S}_c(\omega)$ is required. Assuming the modes are well separated, the spectral moments for the reduced model are calculated using [51]:

$${}_r m_i = 2 \int_0^\infty \omega^i \, {}_r S_c(\omega) \, \mathrm{d}\omega, \tag{20}$$

where the index r is used to describe the participation of a particular mode shape (for details, see [10]). The spectral moments of the individual mode shapes are then summed for the reduced spectral moment:

$$\widetilde{m}_i = \sum_{r=1}^{M} {}_r m_i. \tag{21}$$

Based on the computed spectral moments, damage intensity for the broadband random process can be determined using one of the methods available, *e.g.*, the Tovo–Benasciutti method [62], which defines a linear relation between the broadband damage intensity d_{TB} and narrowband damage estimator d_{NB} [63]. It is defined by the equation:

$$d_{\mathrm{TB}} = \left[b + (1-b)\, \alpha_2^{k-1} \right] \alpha_2 \, d_{\mathrm{NB}}, \tag{22}$$

where b is a broadband weighing parameter, approximated using the spectral moments [13]. α_i is a spectral width parameter [51]. For the broadband weighing parameter b, the following approximation was used [13]:

$$b_{\mathrm{app}}^{\mathrm{TB}} = \frac{(\alpha_1 - \alpha_2)\left[1.112\left(1 + \alpha_1\alpha_2 - (\alpha_1 + \alpha_2)\right) \mathrm{e}^{2.11\alpha_2} + (\alpha_1 - \alpha_2)\right]}{(\alpha_2 - 1)^2} \tag{23}$$

3. Application of thermoelasticity in multiaxial vibration-fatigue criterion

This section introduces the thermoelasticity-based multiaxial vibration-fatigue criterion that has the advantage of being directly measured using a high-speed thermal imaging camera. One of the goals of this research is to determine the validity of the thermoelasticity-based multiaxial criterion in comparison with the EVMS.

Thermoelasticity relies on the sum of the normal stress amplitudes. Based on Eqs. (10) and (11), the formulation for determining the response stress amplitudes of a MDOF system is:

$$\mathbf{X}^s = \mathbf{H}_{sf}(\omega)\, \mathbf{F} = \sum_{r=1}^{N} \frac{{}_r\mathbf{A}_s}{\omega_r^2 - \omega^2 + \mathrm{i}\,\eta_r\,\omega_r^2}\, \mathbf{F} \tag{24}$$

Expressing the modal constant matrix ${}_r\mathbf{A}_s$ with all the components (12), the following matrix equation is obtained, where only the contribution of a single mode r is considered for the purpose of a simple derivation.

$$\begin{bmatrix} \sigma_{xx} \\ \sigma_{yy} \\ \sigma_{zz} \\ \sigma_{xy} \\ \sigma_{xz} \\ \sigma_{yz} \end{bmatrix} = \zeta(\omega) \begin{bmatrix} \phi_{\sigma_{xx}}\phi_x & \phi_{\sigma_{xx}}\phi_y & \phi_{\sigma_{xx}}\phi_z \\ \phi_{\sigma_{yy}}\phi_x & \phi_{\sigma_{yy}}\phi_y & \phi_{\sigma_{yy}}\phi_z \\ \phi_{\sigma_{zz}}\phi_x & \phi_{\sigma_{zz}}\phi_y & \phi_{\sigma_{zz}}\phi_z \\ \phi_{\sigma_{xy}}\phi_x & \phi_{\sigma_{xy}}\phi_y & \phi_{\sigma_{xy}}\phi_z \\ \phi_{\sigma_{xz}}\phi_x & \phi_{\sigma_{xz}}\phi_y & \phi_{\sigma_{xz}}\phi_z \\ \phi_{\sigma_{yz}}\phi_x & \phi_{\sigma_{yz}}\phi_y & \phi_{\sigma_{yz}}\phi_z \end{bmatrix} \begin{bmatrix} f_x \\ f_y \\ f_z \end{bmatrix} \tag{25}$$

$\zeta(\omega)$ represents the dynamic part of the equation:

$$\zeta(\omega) = \frac{1}{\omega_r^2 - \omega^2 + \mathrm{i}\eta_r\omega_r^2} \tag{26}$$

Inserting the stress components from Eq. (25) into the thermoelastic law (2), the thermoelastic effect for a single mode system can be expressed, where the normal stress amplitudes are summed and the shear stress amplitudes are neglected:

$$\Delta T / K_m = \sigma_{xx} + \sigma_{yy} + \sigma_{zz} = \zeta(\omega) \left(\phi_{\sigma_{xx}} + \phi_{\sigma_{yy}} + \phi_{\sigma_{zz}} \right) \left(f_x \phi_x + f_y \phi_y + f_z \phi_z \right) \tag{27}$$

Eq. (27) shows, how the thermoelastic effect (the sum of the normal stress amplitudes) can be calculated and related to the temperature change ΔT. However, in vibration-fatigue analysis, the PSDs of the stress response are needed (not the amplitudes) (20).

The equivalent stress PSD of the thermoelastic criterion cannot be simply calculated as a sum of the normal stress PSD components (auto-spectral densities), as they are positive values by definition and do not include the phase or sign information. On the other hand, the thermoelastic criterion relies on the sum of the normal stress amplitudes (not the PSD), considering their signs (2), resulting in the negative (compressive) and positive (tensile) stresses being subtracted. This means that the thermoelastic criterion needs to be reformulated for use in the frequency domain.

Similar to the EVMS criterion formulation (17), the proposed thermoelasticity-based criterion is defined with the constants matrix $\mathbf{Q}$. In this case, a thermoelastic criterion matrix that sums the normal stresses in the PSD formulation is:

$$\mathbf{Q}_{\text{thermo}} = \begin{bmatrix} 1 & 1 & 1 & 0 & 0 & 0 \\ 1 & 1 & 1 & 0 & 0 & 0 \\ 1 & 1 & 1 & 0 & 0 & 0 \\ 0 & 0 & 0 & 0 & 0 & 0 \\ 0 & 0 & 0 & 0 & 0 & 0 \\ 0 & 0 & 0 & 0 & 0 & 0 \end{bmatrix}, \tag{28}$$

The $\mathbf{Q}_{\text{thermo}}$ matrix is used in Eq. (17). For a single mode:

$${}_r S_{\text{thermo}}(\omega) = \text{Trace} \left[\mathbf{Q}_{\text{thermo}} \cdot {}_r \mathbf{S}_{ss}(\omega) \right], \tag{29}$$

Inserting ${}_r \mathbf{S}_{ss}$ (16) into Eq. (29):

$${}_r S_{\text{thermo}}(\omega) = \underbrace{\left(\frac{\Delta T}{K_m} \right)^2}_{\text{camera}} = \underbrace{\text{Trace} \left[\mathbf{Q}_{\text{thermo}} \cdot \zeta(\omega) \, {}_r \mathbf{A}_s \, \mathbf{S}_{ff}(\omega) \, {}_r \mathbf{A}_s^{*\,\text{T}} \right]}_{\text{simulation}} \tag{30}$$

Considering Eq. (30) in components notation, the formulation can be simplified to the thermoelasticity-based equivalent uniaxial stress PSD:

$${}_r S_{\text{thermo}}(\omega) = \underbrace{\left(\frac{\Delta T}{K_m} \right)^2}_{\text{camera}} = \underbrace{\left(\zeta(\omega) \left(\phi_{\sigma_{xx}} + \phi_{\sigma_{yy}} + \phi_{\sigma_{zz}} \right) \left(f_x \phi_x + f_y \phi_y + f_z \phi_z \right) \right)^2}_{\text{simulation}} \tag{31}$$

On one hand, the thermoelasticity-based equivalent stress ${}_r S_{\text{thermo}}(\omega)$ can be determined with a numerical simulation, as a response to the given excitation PSD. Based on the thermoelasticity-based equivalent stress, the spectral moments and damage are computed, as described in Section 2.4 (instead of ${}_r S_c(\omega)$ the ${}_r S_{\text{thermo}}(\omega)$ has to be used). Details are given in the numerical experiment (Section 4.1), which compares the proposed thermoelasticity-based uniaxial equivalent to the EVMS (17) criterion.

On the other hand, the equivalent stress ${}_r S_{\text{thermo}}(\omega)$ can be measured directly with the thermal imaging camera, as shown with the underbraces in Eqs. (30) and (31). As the thermal camera measures the temperature/stresses on the surface of structures, the formulation for the thermoelastic effect can be simplified for the plane-stress (*i.e.*, $\Delta\sigma_3 = 0$) [44]. Expressing Eq. (2) for plane-stress and in principal stress notation:

$$\Delta T = K_m \left(\Delta\sigma_1 + \Delta\sigma_2 \right), \tag{32}$$

meaning, that out of the established multiaxial criteria [59], the thermoelasticity-based criterion is the most similar to the maximum principal stress criterion. The thermoelastic criterion on the surface ($\Delta\sigma_1 + \Delta\sigma_2$) is only different from the maximum principal stress ($\Delta\sigma_1$) by the amplitude of the second principal stress $\Delta\sigma_2$, which is smaller than $\Delta\sigma_1$ by definition. The thermoelasticity-based criterion is valid when the surface shear stresses are negligible (no in-plane or out-of-plane shear).

4. Experimental research

To compare the thermoelastic multiaxial criterion to the EVMS, a numerical FEM experiment is discussed in Section 4.1 followed by a real experiment in Section 4.2.

4.1. Numerical experiment

A FEM model of the aluminium Y-shaped specimen [64] shown in Fig. 1 is used. The model is excited using a random uniform broadband excitation $\mathbf{S}_{ff,z}(\omega)$ along the z-axis, exciting the first six modes $r = 1, 2, \ldots, 6$. The model is fixed on the bottom side in x and y-axis, which simulates the specimen fixed to the shaker with the vertical motion free (z-axis). The first six eigenmodes are calculated using the open-source software SfePy [65]. The eigenfrequencies are given in Table 1.

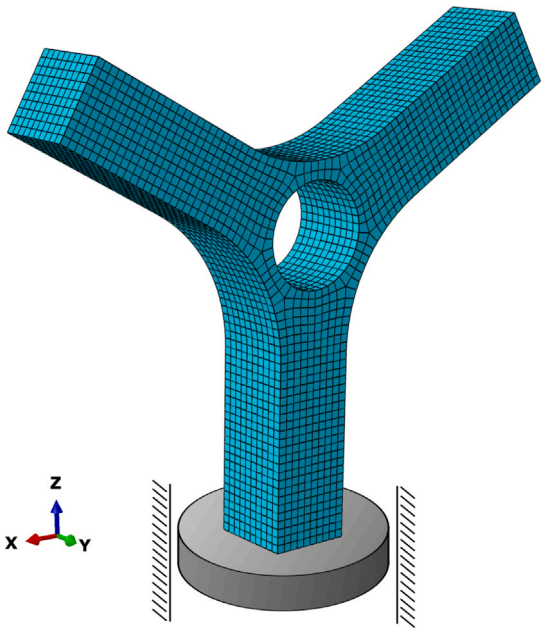

Fig. 1. Y-Sample mesh and boundary conditions.

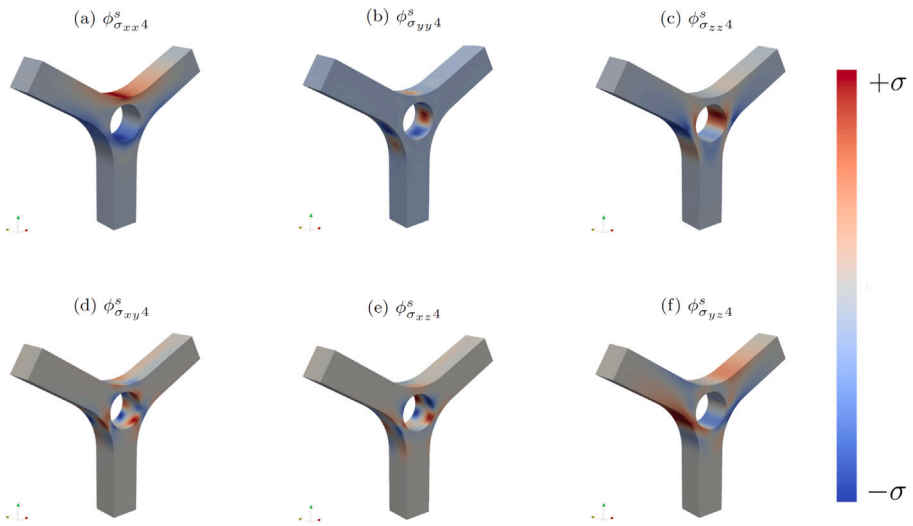

Fig. 2. Stress mode shape components for the fourth mode $\omega_4 = 6846$ Hz. Stress is normalized to the maximum and minimum of each stress component.

Table 1
Eigenfrequencies of the numerical model (clamped, free in z-direction).

ω_r [Hz]	1600	3831	6556	6846	11 410	15 840

From the 6 displacement mode shapes ϕ_r, the six stress mode shapes ϕ^s_r are also calculated, as shown in Eq. (9).

Each of the six stress modes has six stress components. In Fig. 2, the stress components of the fourth stress mode ϕ^s_4 are shown. As the mode shapes have no units, each of the plots in Fig. 2 is normalized to its maximum value.

The EVMS and the thermoelastic criterion are used as described in Section 3 to calculate the uniaxial equivalent stress response. To analyse the extent, to which the shear stresses are present in the model, the thermoelastic equivalent stress (29) is compared to the largest shear-stress component in the same colour range 3. It can be observed that in this model the maximum shear-stress component is approximately 10 times smaller than the sum of the normal stresses, used in thermoelastic criterion, meaning, that the assumption of the small shear stresses is valid in this case.

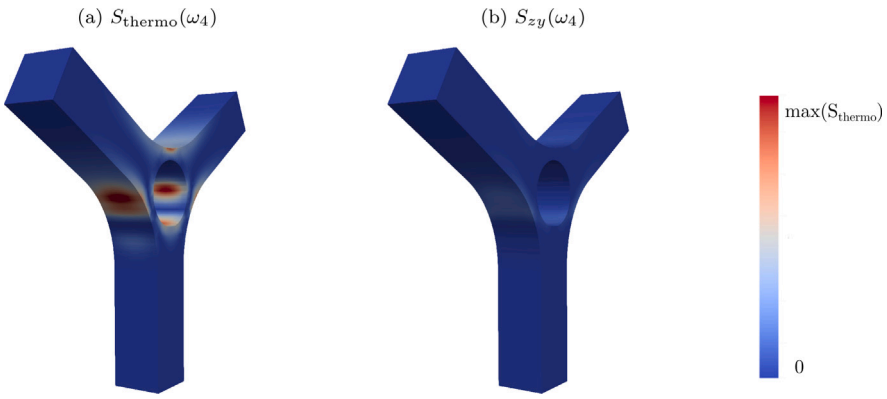

Fig. 3. Numerical results at 4th natural frequency: (a) uniaxial equivalent stress response $S_{\text{thermo}}(\omega_4)$ vs (b) shear stress $S_{zy}(\omega_4)$. Scale is normalized to max of $S_{\text{thermo}}(\omega_4)$.

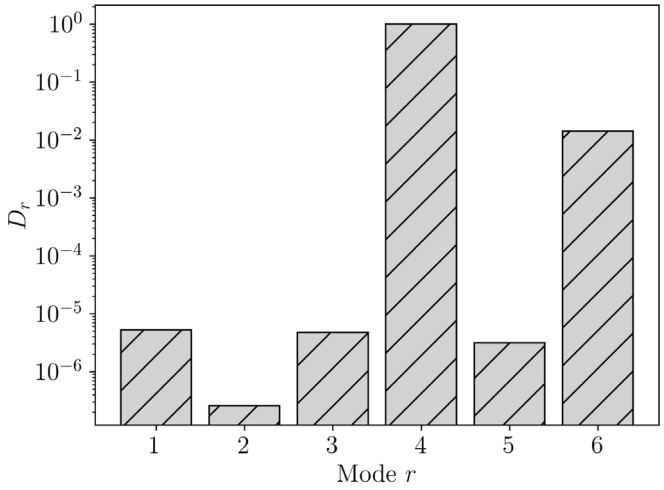

Fig. 4. Damage contribution of the specific modes.

The spectral moments are then calculated for each mode of both response PSDs. Eq. (20) can be simplified for the case of uniform excitation acting only in the z-direction [10]:

$$ {}_r m_i = \underbrace{2 \cdot \int_0^{\infty} \omega^i \, \zeta(\omega) \, \mathrm{d}\omega}_{{}_r I_i} \cdot \mathrm{Trace}\left[\mathbf{Q} \cdot {}_r\mathbf{A}_s \cdot \mathbf{S}_{ff,z} \cdot {}_r\mathbf{A}_s^{*\,\mathrm{T}}\right] \tag{33} $$

The integral ${}_r I_i$ only needs to be calculated once for each mode r, and once for each order of the spectral moment i. All the moments are summed for the complete reduced model (21). The Tovo–Benasciutti method is used to determine the damage intensity (22).

The mode-damage contribution was calculated, as by Mršnik et al. [10], using the EVMS. A measure of the damage intensity D_r is determined, which represents the effect a single mode has on the total damage intensity d. To determine D_r, the partial damage intensity $d_{\setminus M_r}$ is calculated using all the modes with the exception of mode r. It is then subtracted from the total damage intensity d [10]:

$$ D_r = \frac{d - d_{\setminus M_r}}{d} = 1 - \frac{d_{\setminus M_r}}{d} \tag{34} $$

It was discovered that the fourth eigenmode $\omega_4 = 6846$ Hz contributes the most to the damage intensity, as shown in Fig. 4. Note that the damage contribution in Fig. 4 is on a logarithmic scale.

The damage intensity using the EVMS and the thermoelastic criterion is displayed in Fig. 5. The thermoelastic criterion estimates the damage in the critical point approximately 50% higher than the EVMS.

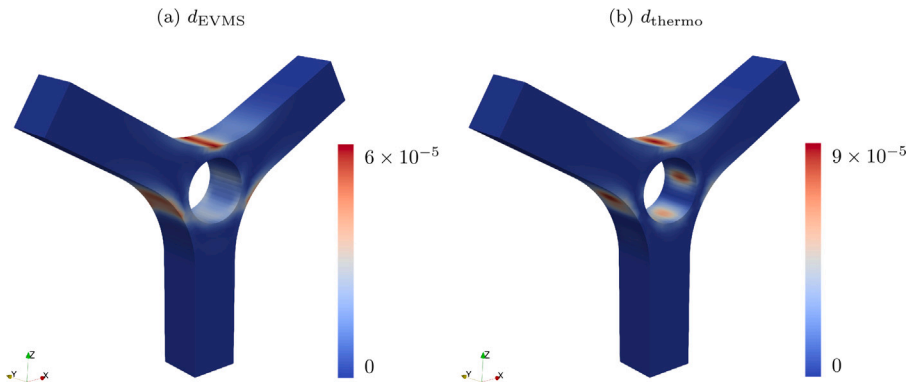

Fig. 5. Damage, determined using (a) EVMS and (b) thermoelastic criterion.

4.2. Real experiment

An experiment with a thermal camera was conducted to further research the numerical experiment and to compare the simulated damage intensity to the measured thermoelastic effect.

The same Y-shaped aluminium specimen as used in the numerical experiment (Fig. 1) was clamped vertically to the head of an electro-dynamic shaker (model LDS V555). The Telops FAST m3K high-speed thermal imaging camera was positioned as shown in Fig. 6. The specimen was painted with a high-emissivity, low-reflectivity black paint, to maximize the visibility of the thermoelastic effect, and minimize the IR reflections from the environment that could be falsely identified as thermoelasticity. To further reduce any IR reflections, an absorbing material was placed behind the specimen, resulting in the specimen being better distinguishable from the background in the video. To decrease the eigenfrequencies to where they are measurable with the thermal camera, two 200 g weights were mounted on the arms of the Y-specimen, as shown in Fig. 6(b). With the added masses, the fourth eigenfrequency, previously $\omega_4 = 6846$ Hz, is reduced to $\omega_4 = 313$ Hz. Although the weights cause an overall increase of the stresses on the specimen, it is assumed that the relative distribution of the stresses in the fatigue zone and the location of the critical points are not qualitatively influenced by the weights. As it was discovered in numerical experiment, the fourth mode shape contributes the most to the damage, see Fig. 4. In the real experiment with the thermal camera, only the fourth mode was excited with the purpose of increasing the signal-to-noise ratio of the measurement, as the thermoelastic effect in structural dynamics is typically at the level of millikelvin, which is near the sensibility of the camera. To excite the fourth mode shape, the specimen was excited with a random signal from 300 to 330 Hz.

Thermal camera measurement.

A Telops FAST m3K high-speed thermal camera was used to capture the thermoelastic effect on the surface of the specimen. The camera was set to a resolution of 132×128 pixels and 5000 FPS (Frames Per Second). The camera uses 16-bit encoding and has a Noise Equivalent Temperature Difference (NETD) [66] of 32 mK. The length of the measurement was set to 5 s. A Fourier transformation was used to convert the temperature-variation measurement at each pixel into the frequency domain. Averaging of a subset size 3×3 around the pixel of interest was used to improve the signal-to-noise ratio of the measurement.

The thermoelastic effect at $\omega_4 = 313$ Hz was clearly visible in the frequency domain. By mapping the amplitudes of the temperature variation of the observed mode shape to every pixel, the heatmaps shown in Figs. 7 and 8 are generated.

In Fig. 7, the results from the FEM analysis and the thermal camera measurement are compared. In Fig. 7(a), the simulated first invariant of the fourth mode shape is displayed ($\phi_{\sigma_{xx}4} + \phi_{\sigma_{yy}4} + \phi_{\sigma_{zz}4}$) (31). Fig. 7(b) shows the same stress response, measured with a thermal camera, when exciting the fourth mode shape. This stress response is proportional to the first invariant of the stress mode shape, as shown in Eq. (31). In Fig. 7(b), the imaginary component of the measurement is shown, with the purpose of also displaying the sign of the temperature's amplitude.

Fig. 8 shows the differences between the calculated damage intensity using the EVMS criterion and the proposed thermoelastic criterion in comparison with the damage calculated using the thermoelastic effect, measured with the thermal camera.

5. Discussion

In the synthetic experiment the damage intensities of the model were calculated using the established EVMS method and the proposed thermoelasticity-based method. By comparing the results, it is possible to assess the extent to which the thermoelastic criterion is close to the EVMS. Further, the numerical experiment is used to investigate whether the analysis of the multiaxial vibration fatigue based on the thermal imaging camera is reasonable. The results of the numerical experiment are also compared with a real thermoelastic effect measured with a thermal imaging camera.

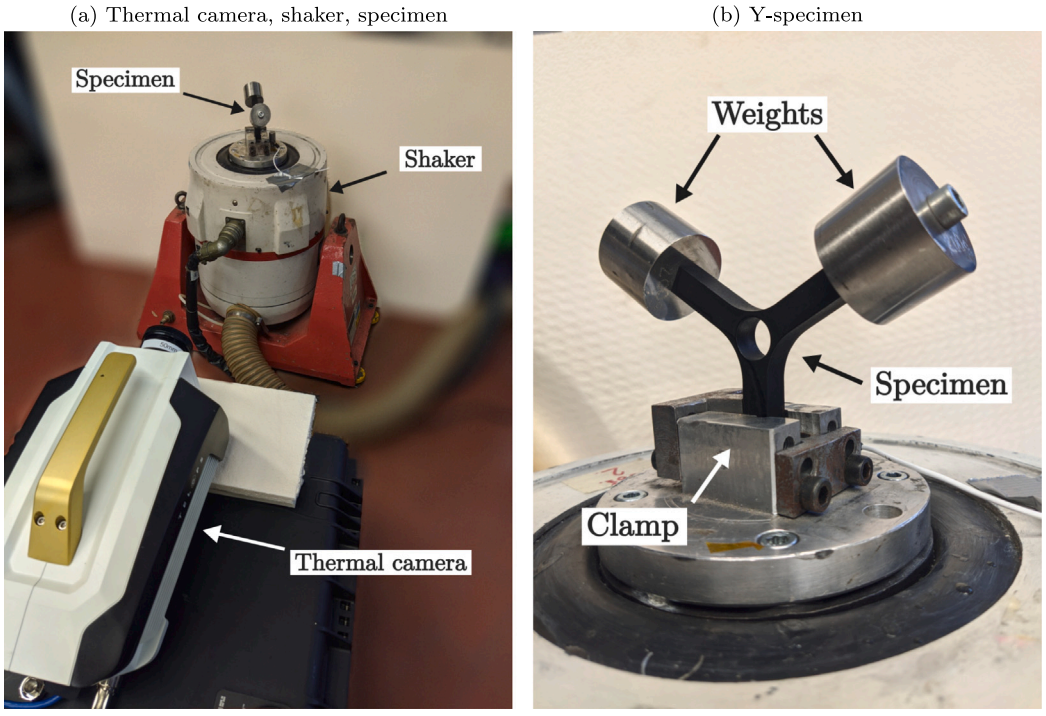

Fig. 6. Experimental setup.

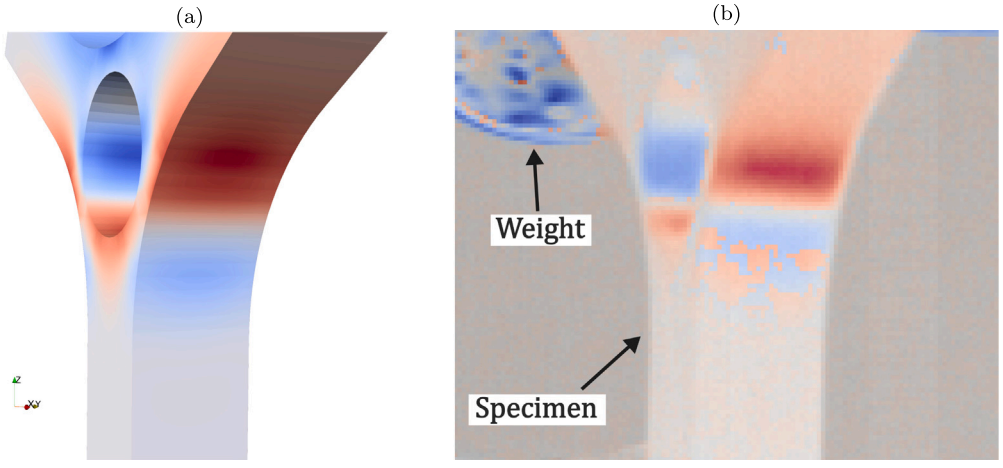

Fig. 7. Comparison of (a) simulated stress mode shape (first invariant) $\phi_{\sigma_{xx}4} + \phi_{\sigma_{yy}4} + \phi_{\sigma_{zz}4}$ and (b) measured stress response at the fourth natural frequency.

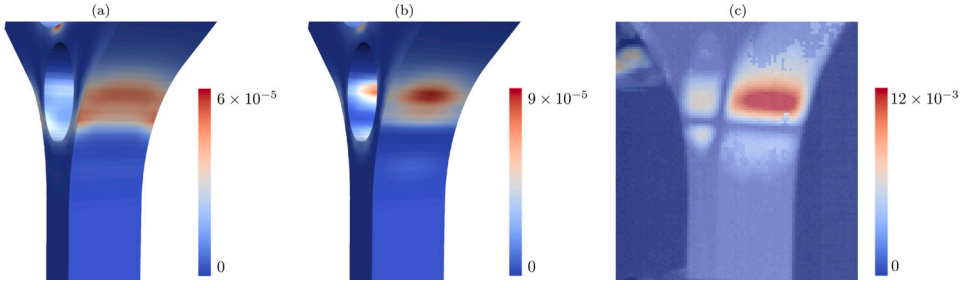

Fig. 8. Comparison of calculated damage intensity by (a) EVMS FEM: d_{EVMS}, (b) thermoelastic criterion FEM: d_{thermo} and (c) measured thermoelastic effect.

For a Y-sample, Fig. 7 shows the first invariant of the fourth stress mode shape in comparison with the experimentally measured thermoelastic response, when narrowband excited close to the fourth natural frequency. The results of the FEM modal analysis and the experiment with the thermal camera show a good correlation, as the measured distribution of the tensile and compressive stresses is clearly proportionate to the FEM simulation.

It is essential to verify the locations of the damage-critical points on the model, as this is the key information for the damage-reasoning analysis in real-world applications. Comparing the locations of critical points in Fig. 8, it can be observed that the EVMS and the thermoelasticity-based criterion give similar results, *i.e.*, critical points are on the thinnest section of the model/experiment around the central hole. While the location of the critical points shows good alignment, the distribution of the damage intensity around them differs. The damage intensity, calculated using the EVMS (Fig. 8a), is more evenly distributed across the whole side cross-section of the model, while the thermoelastic criterion gives a localization of the damage intensity at the centre, with an oval-shaped distribution around it (Fig. 8b). The difference in results is caused by the fact that the thermoelastic criterion does not consider the shear stresses, unlike the EVMS, which considers the full stress tensor. The shear stresses are predominant near the edges of the model in this case, like it can be observed in Fig. 2, while the normal stresses have their maximum near the centre of the cross-section.

Comparing the thermoelastic effect heatmap measured with the thermal camera (Fig. 8c) with the FEM result (Fig. 8b), it is evident that the simulated critical points match the measured hotspots of the thermoelastic effect. The distribution of the measured amplitudes has a distinct oval shape with a maximum in the centre, which resembles the damage intensity computed using the thermoelastic criterion. The damage measured with the thermal camera is higher than the simulated damage because of the added weights in the experiment.

6. Conclusions

Based on minute changes in the surface temperature, the thermoelasticity enables full-field, close-to-real-time and non-contact stress-state measurements of dynamically excited structures. When measuring multiaxial stress states, the thermal camera inherently acts as a multiaxial criterion as it identifies the uniaxial equivalent stress (scalar value) on the surfaces of the structures. Under the adiabatic conditions, the temperature oscillations are directly proportionate to the first invariant of the stress tensor (sum of the normal stresses). The temperature oscillations can be measured with a fast thermal imaging camera and related to the first stress invariant through the material's thermoelastic constant and directly used for damage-intensity identification. The second stress invariant (related to shear stresses) cannot be detected with a thermal camera.

This research introduces the thermoelasticity-based multiaxial vibration fatigue criterion as an alternative to the established methods (*e.g.*, EVMS criterion). The advantage of the thermoelastic criterion is the ability for its direct identification with a thermal camera, as there is currently no other method for the full-field multiaxial damage detection. The research introduces the definition of the thermoelastic multiaxial vibration-fatigue criterion, which is used for simulating results similar to those measured with a thermal camera during harmonic excitation. The damage, calculated with the proposed thermoelastic criterion, is compared to the EVMS in a numerical experiment.

The limitations of the thermoelastic approach are showcased. The proposed thermoelasticity-based damage identification can only be applied if the normal stresses are much bigger than the shear stresses. Since the thermal camera measures the first stress invariant, it cannot detect shear stresses, limiting its applicability in certain multiaxial stress conditions. However, normal stresses still play a crucial role in fatigue crack initiation in many cases, such as bending, where cyclic tension and compression occur. Thus, while the criterion is not suited for all scenarios, it is highly effective in cases where normal stresses dominate. Comparing the damage calculated with the EVMS and the thermoelastic criterion on the Y-shaped model, the general location of the critical points coincides. The observed differences were due to the fact that the thermoelastic criterion overestimates the damage in comparison with the EVMS under biaxial tension or biaxial compression and underestimates the damage when the principal stresses on the surface have different signs, with zero damage being detected under pure shear stress ($\sigma_1 = -\sigma_2$).

As the proposed criterion is related to the first stress invariant, it is independent of the principal axis orientation, meaning it has the same value under rotating principal directions. By the categorization of numerical models, defined by Skibicki [67], the thermoelasticity based criterion falls under the category of models which, technically speaking, allow calculations for non-proportional loading, but do not take into account the influence of non-proportionality on fatigue life or strength.

The simulated vibration-fatigue damage of the Y-sample is compared to a real experiment. The vibration-fatigue damage experimentally identified at fourth mode shape corresponds to the one numerically simulated. The experiment shows that real-time and full-field experimental identification of vibration-fatigue damage is possible. Based on the proposed approach, a new insight into vibration-fatigue damage is possible, potentially fostering new research in understanding the mechanisms of multiaxial damage.

CRediT authorship contribution statement

Jaša Šonc: Writing – original draft, Visualization, Validation, Software, Methodology, Investigation, Formal analysis, Data curation. **Klemen Zaletelj:** Writing – review & editing, Writing – original draft, Visualization, Validation, Software, Resources, Project administration, Methodology, Investigation, Formal analysis, Data curation, Conceptualization. **Janko Slavič:** Writing – review & editing, Writing – original draft, Validation, Supervision, Resources, Project administration, Methodology, Investigation, Funding acquisition, Data curation, Conceptualization.

Declaration of competing interest

The authors declare that they have no known competing financial interests or personal relationships that could have appeared to influence the work reported in this paper.

Data availability

Data will be made available on request.

Acknowledgements

The authors acknowledge partial financial support from the Slovenian Research Agency (research core funding No. P2-0263).

Appendix. Thermoelasticity

The laws of the thermoelastic effect are based on the laws of thermodynamics [68] and the laws of continuum mechanics [69]. From the first and second laws of thermodynamics, the expression is derived [39]:

$$\mathrm{d}u = \delta q + \delta w, \tag{A.1}$$

where u is the internal energy, q is the heat transferred from the surroundings to the system and w is the work exchanged with the surroundings. The following relations define the work w and the entropy s in differential form [68]:

$$\delta w = \frac{\sigma_{ij}\,\mathrm{d}\varepsilon_{ij}}{\rho}, \tag{A.2}$$

$$\mathrm{d}s = \frac{\delta q}{T}, \tag{A.3}$$

where σ_{ij} and ε_{ij} are the stress and the deformation tensors and ρ is the material density [48]. Using relations (A.2) and (A.3), Eq. (A.1) becomes:

$$\mathrm{d}u = T\,\mathrm{d}s + \frac{\sigma_{ij}\,\mathrm{d}\varepsilon_{ij}}{\rho}, \tag{A.4}$$

To derive the thermoelastic law, the Helmholtz free energy H is introduced in its differential form [46]:

$$\mathrm{d}H = \mathrm{d}u - T\,\mathrm{d}s - s\,\mathrm{d}T \tag{A.5}$$

Inserting Eq. (A.1) into Eq. (A.5), the following expression is derived, where the assumption of local reversible changes is used:

$$\mathrm{d}H = \frac{\sigma_{ij}\,\mathrm{d}\varepsilon_{ij}}{\rho} - s\,\mathrm{d}T \tag{A.6}$$

The Helmholtz free energy H can also be defined as a state function, *i.e.*, as two partial derivatives, first, at constant temperature and second, at constant deformation [46]:

$$\mathrm{d}H = \left(\frac{\partial H}{\partial \varepsilon_{ij}}\right)_T \mathrm{d}\varepsilon_{ij} + \left(\frac{\partial H}{\partial T}\right)_{\varepsilon_{ij}} \mathrm{d}T \tag{A.7}$$

By comparing Eqs. (A.6) and (A.7), the following relations are obtained [46]:

$$\sigma_{ij} = \rho\frac{\partial H}{\partial \varepsilon_{ij}} \tag{A.8}$$

$$s = -\frac{\partial H}{\partial T} \tag{A.9}$$

The entropy s can also be defined as a state function of deformation and temperature:

$$\mathrm{d}s = \left(\frac{\partial s}{\partial \varepsilon_{ij}}\right)_T \mathrm{d}\varepsilon_{ij} + \left(\frac{\partial s}{\partial T}\right)_{\varepsilon_{ij}} \mathrm{d}T \tag{A.10}$$

From (A.3) and (A.9), the specific heat per unit mass at zero strain c_ε is introduced to derive the thermoelastic law:

$$c_\varepsilon = \left(\frac{\delta q}{\mathrm{d}T}\right)_{\varepsilon_{ij}} = \left(\frac{T\,\mathrm{d}s}{\mathrm{d}T}\right)_{\varepsilon_{ij}} = -T\left(\frac{\partial^2 H}{\partial T^2}\right)_{\varepsilon_{ij}} \tag{A.11}$$

Inserting Eqs. (A.8), (A.9) and (A.11) into Eq. (A.10), results in [46]:

$$\mathrm{d}s = -\frac{1}{\rho}\frac{\partial \sigma_{ij}}{\partial T}\,\mathrm{d}\varepsilon_{ij} + c_\varepsilon\frac{\mathrm{d}T}{T} \tag{A.12}$$

From the definition of entropy (A.3) and Eq. (A.12), it follows:

$$\frac{\delta q}{T} = -\frac{1}{\rho}\frac{\partial \sigma_{ij}}{\partial T}\,\mathrm{d}\varepsilon_{ij} + c_\varepsilon\frac{\mathrm{d}T}{T} \tag{A.13}$$

Finally, expressing $\mathrm{d}T$, Eq. (A.13) becomes:

$$\mathrm{d}T = \frac{T}{\rho\, c_\varepsilon}\frac{\partial \sigma_{ij}}{\partial T}\,\mathrm{d}\varepsilon_{ij} + \frac{\delta q}{c_\varepsilon} \tag{A.14}$$

From the laws of thermodynamics, Eq. (A.14) is derived, which gives the relation between temperature change and both the stress and strain tensors. To define the relation between the temperature change and the stress, the strain tensor must be related to the stress tensor using constitutive relations [69]:

An equation that relates the strain tensor to the stress tensor can be written in the following way:

$$\sigma_{ij} = 2\,\mu\,\varepsilon_{ij} + \left(\lambda\,\varepsilon_{kk} - \gamma\,\Delta T\right)\delta_{ij}\,, \tag{A.15}$$

Eq. (A.15) is valid for homogenous isotropic conditions and μ, λ and γ are Lamé parameters [70]. δ_{ij} is the Kronecker delta defined as:

$$\delta_{ij} = \begin{cases} 1 & \text{if } i = j \\ 0 & \text{if } i \neq j \end{cases} \tag{A.16}$$

From Eqs. (A.15) and (A.16) it is evident that the temperature changes are only related to diagonal values of the stress tensor, *i.e.*, the normal stresses [70]. Combining Eq. (A.14) and constitutive relation (A.15) results in:

$$\frac{\partial \sigma_{ij}}{\partial T} = -\gamma\,\delta_{ij}\,, \tag{A.17}$$

Eq. (A.17) can be inserted into Eq. (A.10):

$$\mathrm{d}s = c_\varepsilon\frac{\mathrm{d}T}{T} + \frac{\gamma}{\rho}\delta_{ij}\,\mathrm{d}\varepsilon_{ij} \tag{A.18}$$

The product of δ_{ij} and $\mathrm{d}\varepsilon_{ij}$ is ε_{kk}, which is the first invariant of the strain tensor or cubic dilatation [69]:

$$\mathrm{d}s = c_\varepsilon\frac{\mathrm{d}T}{T} + \frac{\gamma}{\rho}\mathrm{d}\varepsilon_{kk} \tag{A.19}$$

By integrating Eq. (A.19) and considering the initial conditions $s_v = 0$, $(\epsilon_{ij})_0 = \epsilon_{ij}$ in $T = T_0$, the following equation is obtained (assuming small temperature differences $\Delta T \ll T_0$ [40]):

$$s = c_\varepsilon\frac{\Delta T}{T_0} + \frac{\gamma}{\rho}\Delta\varepsilon_{kk} \tag{A.20}$$

Considering an adiabatic process, $s = 0$, Eq. (A.20) becomes:

$$\Delta\varepsilon_{kk} = -\frac{\Delta T}{\gamma\, T_0}\rho\, c_\varepsilon \tag{A.21}$$

By using the constitutive relation in Eq. (A.15), Lamé constants and defining the relation between the heat capacities at constant pressure c_p and zero strain c_ε (for more details see [46]), the law of the thermoelastic effect is derived:

$$\Delta\sigma_{kk} = -\Delta T\,\frac{\rho}{\alpha\, T_0}c_p \tag{A.22}$$

or:

$$\Delta T = K_m\left(\Delta\sigma_{xx} + \Delta\sigma_{yy} + \Delta\sigma_{zz}\right) \tag{A.23}$$

where K_m is the thermoelastic constant [48]:

$$K_\mathrm{m} = -\frac{\alpha\, T_0}{\rho\, c_\mathrm{p}} \tag{A.24}$$

T_0 is the temperature of the surroundings and α is a coefficient of heat expansion.

References

[1] Matjaž Mršnik, Janko Slavič, Miha Boltežar, Multiaxial vibration fatigue—A theoretical and experimental comparison, Mech. Syst. Signal Process. 76 (2016).

[2] Denis Benasciutti, Frank Sherratt, Alessandro Cristofori, Basic principles of spectral multi-axial fatigue analysis, Procedia Eng. 101 (2015) 34–42, 3rd International Conference on Material and Component Performance under Variable Amplitude Loading, VAL 2015.

[3] Matjaž Mršnik, Janko Slavič, Miha Boltežar, Frequency-domain methods for a vibration-fatigue-life estimation – application to real data, Int. J. Fatigue 47 (2013) 8–17.

[4] Ronghui Zheng, Jinpeng Li, Huaihai Chen, Investigation of planar translational and rotational stationary non-Gaussian random vibration test, Mech. Syst. Signal Process. 191 (2023) 110186.

[5] Arvid Trapp, Peter Wolfsteiner, Estimating higher-order spectra via filtering-averaging, Mech. Syst. Signal Process. 150 (2020).

[6] Guiwei Zhang, Weiguang Li, Xiaochen Wang, Zhichun Yang, Influence of flexible structure vibration on the excitation forces delivered by multiple electrodynamic shakers, Mech. Syst. Signal Process. 169 (2022) 108753.

[7] Michele Sgamma, Massimiliano Palmieri, Michele Barsanti, Francesco Bucchi, Filippo Cianetti, Francesco Frendo, Study of the response of a single-DoF dynamic system under stationary non-Gaussian random loads aimed at fatigue life assessment, Heliyon (2024).

[8] Giacomo D'Elia, Emiliano Mucchi, Giorgio Dalpiaz, A novel methodology for dynamic response maximisation in multi-axis accelerated random fatigue testing, Mech. Syst. Signal Process. 181 (2022) 109491.

[9] Arvid Trapp, David Fräulin, Marcin Hinz, Peter Wolfsteiner, Data-driven spectral damage estimator for non-stationary vibration loading, Procedia Struct. Integr. 54 (2024) 521–535.

[10] Matjaž Mršnik, Janko Slavič, Miha Boltežar, Vibration fatigue using modal decomposition, Mech. Syst. Signal Process. 98 (2018) 548–556.
[11] Claudio Braccesi, Filippo Cianetti, Lorenzo Tomassini, An innovative modal approach for frequency domain stress recovery and fatigue damage evaluation, Int. J. Fatigue 91 (2016) 382–396, Variable Amplitude Loading.
[12] Turan Dirlik, Application of Computers in Fatigue Analysis (Ph.D. thesis), University of Warwick, 1985.
[13] D. Benasciutti, R. Tovo, Spectral methods for lifetime prediction under wide-band stationary random processes, Int. J. Fatigue 27 (8) (2005) 867–877.
[14] Zhen Gao, Torgeir Moan, Frequency-domain fatigue analysis of wide-band stationary Gaussian processes using a trimodal spectral formulation, Int. J. Fatigue 30 (10) (2008) 1944–1955.
[15] G. Petrucci, B. Zuccarello, Fatigue life prediction under wide band random loading, Fatigue Fract. Eng. Mater. Struct. 27 (12) (2004) 1183–1195.
[16] Wangwen Zhao, Michael J. Baker, On the probability density function of rainflow stress range for stationary Gaussian processes, Int. J. Fatigue 14 (2) (1992) 121–135.
[17] Aleš Zorman, Janko Slavič, Miha Boltežar, Vibration fatigue by spectral methods—A review with open-source support, Mech. Syst. Signal Process. 190 (2023) 110149.
[18] C. Braccesi, G. Morettini, F. Cianetti, M. Palmieri, Evaluation of fatigue damage with an energy criterion of simple implementation, Procedia Struct. Integr. 8 (2018) 192–203, AIAS2017 - 46th Conference on Stress Analysis and Mechanical Engineering Design, 6-9 September 2017, Pisa, Italy.
[19] Dai-yang Gao, Wei-xing Yao, Tao Wu, A damage model based on the critical plane to estimate fatigue life under multi-axial random loading, Int. J. Fatigue 129 (2019) 104729.
[20] Denis Benasciutti, Davide Zanellati, Alessandro Cristofori, The "Projection-by-Projection" (PbP) criterion for multiaxial random fatigue loadings: Guidelines to practical implementation, Frattura ed Integrità Strutturale 47 (2019) 348–366.
[21] Adam Niesł ony, Comparison of some selected multiaxial fatigue failure criteria dedicated for spectral method, J. Theoret. Appl. Mech. 48 (2010) 233–254.
[22] C. Braccesi, F. Cianetti, G. Lori, D. Pioli, Random multiaxial fatigue: A comparative analysis among selected frequency and time domain fatigue evaluation methods, Int. J. Fatigue 74 (2015) 107–118.
[23] Alexander T. Schmidt, Jan Kraft, A new equivalent stress approach based on complex invariants: The COIN LiWI method, Int. J. Fatigue 168 (2023) 107474.
[24] M. Aimé, A. Banvillet, L. Khalij, E. Pagnacco, E. Chatelet, R. Dufour, A framework proposal for new multiaxial fatigue damage and extreme response spectra in random vibrations frequency analysis, Mech. Syst. Signal Process. 213 (2024) 111338.
[25] Guohao Sui, Xinyu Jin, Hongyu Cui, Yahui Zhang, Improvement and test verification of the fatigue response spectrum method, Mech. Syst. Signal Process. 217 (2024) 111519.
[26] A. Preumont, Vincent Piefort, Predicting random high-cycle fatigue life with finite elements, J. Vib. Acoust. 116 (1994) 245–248.
[27] M.H.A. Bonte, A. de Boer, R. Liebregts, Determining the von mises stress power spectral density for frequency domain fatigue analysis including out-of-phase stress components, J. Sound Vib. 302 (1–2) (2007) 379–386.
[28] Alexander T. Schmidt, Nimish Pandiya, Extension of the static equivalent stress hypotheses to linearly vibrating systems using wave interference – The LiWi approach, Int. J. Fatigue 147 (2021) 106103.
[29] Peipei Liu, Zhanxiong Ma, Jinho Jang, Hoon Sohn, Motion magnification-based nonlinear ultrasonic signal enhancement and its application to remaining fatigue life estimation of a steel padeye, Mech. Syst. Signal Process. 200 (2023) 110525.
[30] Chunyan Ao, Baijie Qiao, Meiru Liu, Weidong Zhu, Yuda Zhu, Yanan Wang, Xuefeng Chen, Non-contact full-field dynamic strain reconstruction of rotating blades under multi-mode vibration, Mech. Syst. Signal Process. 186 (2023) 109840.
[31] Tsuchin Chu, W. Ranson, Michael Sutton, Applications of digital-image-correlation techniques to experimental mechanics, Exp. Mech. 25 (1985) 232–244.
[32] Jaka Javh, Janko Slavič, Miha Boltežar, High frequency modal identification on noisy high-speed camera data, Mech. Syst. Signal Process. 98 (2018) 344–351.
[33] Klemen Zaletelj, Janko Slavič, Jaša Šonc, Miha Boltežar, Strain experimental modal analysis of an Euler–Bernoulli beam based on the thermoelastic principle, Mech. Syst. Signal Process. 201 (2023) 110655.
[34] Rick Chartrand, Numerical differentiation of noisy, nonsmooth data, ISRN Appl. Math. 2011 (2011) 1–11.
[35] Richard I. Hartley, Peter Sturm, Triangulation, Comput. Vis. Image Underst. 68 (2) (1997) 146–157.
[36] Domen Gorjup, Janko Slavič, Miha Boltežar, Frequency domain triangulation for full-field 3D operating-deflection-shape identification, Mech. Syst. Signal Process. 133 (2019) 106287.
[37] Richard J. Greene, Eann A. Patterson, Robert E. Rowlands, Thermoelastic stress analysis, in: Springer Handbook of Experimental Solid Mechanics, Springer US, Boston, MA, 2008, pp. 743–768.
[38] J.M. Dulieu-Barton, Introduction to thermoelastic stress analysis, Strain 35 (2) (1999) 35–39.
[39] W. Thompson, On the dynamical theory of heat, Earth Environ. Sci. Trans. R. Soc. Edinb. 20 (2) (1853) 261–288.
[40] M.A. Biot, Thermoelasticity and irreversible thermodynamics, J. Appl. Phys. 27 (3) (1956) 240–253.
[41] Hu Ling, Dejian Meng, Lijun Zhang, Birui Li, An investigation of initial topography on thermoelastic behavior of brake disc under thermal load, Mech. Syst. Signal Process. 200 (2023) 110521.
[42] A. Quinlan, O. Castro, J.M. Dulieu-Barton, Towards assessment of fatigue damage in composite laminates using thermoelastic stress analysis, Compos. C 12 (2023) 100377.
[43] Ángel J. Molina-Viedma, Luis Felipe-Sesé, Elías López-Alba, Francisco A. Díaz, Thermoelastic effect in modal shapes at high frequencies using infrared thermography, Measurement: J. Int. Measur. Confeder. 176 (2021).
[44] Lorenzo Capponi, Janko Slavič, Gianluca Rossi, Miha Boltežar, Thermoelasticity-based modal damage identification, Int. J. Fatigue 137 (2020) 105661.
[45] Adam Niesł ony, Ewald Macha, Spectral Method in Multiaxial Random Fatigue, vol. 33, Springer, Berlin Heidelberg, 2007.
[46] G. Pitarresi, E.A. Patterson, A review of the general theory of thermoelastic stress analysis, J. Strain Anal. Eng. Des. 38 (5) (2003) 405–417.
[47] Charles E. Bakis, Kenneth L. Reifsnider, The adiabatic thermoelastic effect in laminated fiber composites, J. Compos. Mater. 25 (1991) 809–830.
[48] W.N. Sharpe, Springer Handbook of Experimental Solid Mechanics, Springer Science and Business Media, 2008.
[49] N.M.M. Maia, J.M.M. Silva, Theoretical and Experimental Modal Analysis, Research Studies Press, 1997.
[50] D.J. Ewins, Modal testing: Theory, practice and application, in: Mechanical Engineering Research Studies: Engineering Dynamics Series, Wiley, 2009.
[51] Janko Slavič, Matjaž Mršnik, Martin Česnik, Jaka Javh, Miha Boltežar, Vibration Fatigue by Spectral Methods, Elsevier, 2021.
[52] D.B. Li, H.C. Zhuge, B. Wang, The principle and techniques of experimental strain modal analysis, in: Proc of 7th IMAC, 1989, pp. 1285–1289.
[53] Tadej Kranjc, Janko Slavič, Miha Boltežar, A comparison of the strain and the classic experimental modal analysis, J. Vib. Control 7 (2014).
[54] K. Shin, J.K. Hammond, Fundamentals of Signal Processing for Sound and Vibration Engineers, John Wiley & Sons, 2008.
[55] Adam Kal'avskỳ, Adam Niesłony, Róbert Huňady, Influence of PSD estimation parameters on fatigue life prediction in spectral method, Materials 16 (3) (2023) 1007.
[56] A. Palmgren, Die lebensdauer von kugellagern, VDI-Zeitschrift 68 (1924) 339–341.
[57] Miner, A. Milton, Cumulative damage in fatigue, J. Appl. Mech. 12 (3) (2021).
[58] A. Cristofori, R. Tovo, An invariant-based approach for high-cycle fatigue calculation, Fatigue Fract. Eng. Mater. Struct. 32 (2009) 310–324.
[59] A. Carpinteri, A. Spagnoli, S. Vantadori, A review of multiaxial fatigue criteria for random variable amplitude loads, Fatigue Fract. Eng. Mater. Struct. 40 (7) (2017) 1007–1036.

[60] Denis Benasciutti, Frank Sherratt, Alessandro Cristofori, Recent developments in frequency domain multi-axial fatigue analysis, Int. J. Fatigue 91 (2016) 397–413.
[61] Denis Benasciutti, Some analytical expressions to measure the accuracy of the “equivalent von Mises stress” in vibration multiaxial fatigue, J. Sound Vib. 333 (18) (2014) 4326–4340.
[62] R. Tovo, Cycle distribution and fatigue damage under broad-band random loading, Int. J. Fatigue 24 (11) (2002) 1137–1147.
[63] Miles, W. John, On structural fatigue under random loading, J. Aeronaut. Sci. 21 (11) (1954) 753–762.
[64] Martin Cesnik, Janko Slavič, Miha Boltežar, Uninterrupted and accelerated vibrational fatigue testing with simultaneous monitoring of the natural frequency and damping, J. Sound Vib. 331 (2012) 5370–5382.
[65] Robert Cimrman, Vladimír Lukeš, Eduard Rohan, Multiscale finite element calculations in Python using SfePy, Adv. Comput. Math. (2019).
[66] C. Hoffman, R. Driggers, Encyclopedia of Optical and Photonic Engineering, Second Edition (Print) - Five Volume Set, Taylor & Francis, 2015.
[67] Dariusz Skibicki, Phenomena and Computational Models of Non-Proportional Fatigue of Materials, Springer, 2014.
[68] Peter Atkins, The Laws of Thermodynamics: A Very Short Introduction, OUP Oxford, 2010.
[69] Anthony James Merrill Spencer, Continuum Mechanics, Courier Corporation, 2004.
[70] W. Nowacki, Thermoelasticity, second ed., Pergamon, Oxford, 1986.